McGinnity et al. EJNMMI Research (2018) 8:46
https://doi.org/10.1186/s13550-018-0396-2

EJNMMI Research

SHORT COMMUNICATION Open Access

Simplifying [^{18}F]GE-179 PET: are both arterial blood sampling and 90-min acquisitions essential?

Colm J. McGinnity[1,2,3,4*], Daniela A. Riaño Barros[1,2], William Trigg[5], David J. Brooks[6,7], Rainer Hinz[8], John S. Duncan[9,10], Matthias J. Koepp[9,10] and Alexander Hammers[1,2,3,11]

Abstract

Introduction: The NMDA receptor radiotracer [^{18}F]GE-179 has been used with 90-min scans and arterial plasma input functions. We explored whether (1) arterial blood sampling is avoidable and (2) shorter scans are feasible.

Methods: For 20 existing [^{18}F]GE-179 datasets, we generated (1) standardised uptake values (SUVs) over eight intervals; (2) volume of distribution (V_T) images using population-based input functions (PBIFs), scaled using one parent plasma sample; and (3) V_T images using three shortened datasets, using the original parent plasma input functions (ppIFs).

Results: Correlations with the original ppIF-derived 90-min V_Ts increased for later interval SUVs (maximal $\rho = 0.78$; 80–90 min). They were strong for PBIF-derived V_Ts ($\rho = 0.90$), but between-subject coefficient of variation increased. Correlations were very strong for the 60/70/80-min original ppIF-derived V_Ts ($\rho = 0.97$–1.00), which suffered regionally variant negative bias.

Conclusions: Where arterial blood sampling is available, reduction of scan duration to 60 min is feasible, but with negative bias. The performance of SUVs was more consistent across participants than PBIF-derived V_Ts.

Keywords: NMDA, PET, Compartmental modelling, CNS-5161, SUV

Introduction

N-Methyl-D-aspartate (NMDA) receptors for L-glutamate, the major excitatory neurotransmitter in the central nervous system, are ligand- and voltage-gated ion channels [1]. Receptor activation is necessary for learning while abnormal activation is associated with neurological and psychiatric disease [1].

We reported the first-in-human use of the NMDA receptor-selective PET radiotracer, [^{18}F]GE-179 [2], an analogue of the non-competitive antagonist, [^{11}C]CNS-5161 [3]. Quantification of [^{18}F]GE-179 volume of distribution (V_T) was based on 90-min scans and compartmental modelling within regions of interest (ROIs) and using rank-shaping regularisation of spectral analysis (SA) at the voxel level. [^{18}F]GE-179 binding in rats and non-human primates could not be blocked in one recent study [4], but interpretation is complicated by the use of anaesthesia with the NMDA receptor inhibitors isoflurane [5] ± ketamine. We have reported substantial global changes in [^{18}F]GE-179 V_T in patients with focal epilepsy, using "classical" SA [6], which is more widely used than rank-shaping.

Several ongoing studies are using [^{18}F]GE-179 PET. Wide utilisation of [^{18}F]GE-179 is limited by the need for arterial blood sampling and 90-min scans. There is no suitable reference region devoid of NMDA receptors. To facilitate widespread use, we report our investigations into (1) whether arterial blood sampling is avoidable, via the use of standardised uptake values (SUVs) or population-based input functions (PBIFs) and (2) whether shorter scans are feasible.

Materials and methods

Data had been acquired previously after regulatory approvals had been obtained [2, 6]. All participants provided written, informed consent prior to participation.

* Correspondence: colm.mcginnity@kcl.ac.uk
[1]Division of Brain Sciences, Imperial College London, London, UK
[2]MRC Clinical Sciences Centre, London, UK
Full list of author information is available at the end of the article

Springer Open

© The Author(s). 2018 **Open Access** This article is distributed under the terms of the Creative Commons Attribution 4.0 International License (http://creativecommons.org/licenses/by/4.0/), which permits unrestricted use, distribution, and reproduction in any medium, provided you give appropriate credit to the original author(s) and the source, provide a link to the Creative Commons license, and indicate if changes were made.

Arterial blood and dynamic [^{18}F]GE-179 emission scan data were available for nine healthy participants without history of neurological or psychiatric illness and 11 participants with focal epilepsy [2, 6].

Ninety-minute dynamic emission images were acquired using a Siemens/CTI ECAT EXACT HR+ ("962") camera (Knoxville, TN, USA [7]) in 3D mode. Each participant had been injected with a smooth bolus intravenous injection of mean ± standard deviation 187 ± 4 MBq [^{18}F]GE-179, at 30 s after image acquisition commenced. A rotating ^{68}Ge rod source was used to acquire 10-min transmission scans for attenuation and scatter correction, prior to the dynamic emission scans. Continuous arterial blood sampling (5 ml/minute) was performed from 0 to 15 min, and a total of nine discrete arterial blood samples were taken between baseline and 90.5 min post-injection.

MRI and PET image pre-processing

An 83-region grey-matter-only ROI map was produced for each participant using multi-atlas propagation with enhanced registration (MAPER) [8]. MAPER is an automated anatomical segmentation method that involves co-registering the participant's T1-weighted magnetic resonance image (MRI) to that of 30 healthy controls that have already been manually labelled (the atlases). This yields individual anatomical segmentations that are fused via vote-rule decision [9] to produce the ROI map (see Additional file 1: Figure S2).

PET data pre-processing and the generation of parent plasma input functions were performed as previously described [2, 6]. Emission data had been reconstructed using Fourier rebinning (FORE [10]) and 2D-filtered backprojection (FBP; ramp filter kernel 2.0 mm full width at half maximum).

The fraction of plasma radioactivity attributable to the parent [^{18}F]GE-179 had been fitted to a sigmoid function normalised to unity at 0 min using CLICKFIT in-house software version 1.7 (Hinz R, Cunningham VJ, Imaging Research Solutions Limited, London, UK) running in MATLAB 2014a (The MathWorks, Natick, MA, USA.).

The original, continuous parent plasma input functions (ppIFs) were derived as follows [11]: (1) cross-calibration of continuous and discrete whole blood radioactivity concentrations, (2) multiplication of the cross-calibrated continuous (0–15 min) whole blood radioactivity concentrations by the plasma-over-whole-blood ratio, (3) spline interpolation of the continuous (0–15 min) plasma radioactivity concentrations curve over the additional discrete measurements, and (4) multiplication of the continuous (0–90 min) plasma radioactivity curve by the parent fraction.

Voxelwise SA

Voxelwise "classic" SA [12] was performed using Piwave 8.0 [13], using time constants of 5 s (fast boundary = 0.2 s^{-1}) and 5100 s (slow boundary = 0.000196 s^{-1}). We confirmed the suitability of "classic" voxelwise SA by demonstrating that the resultant original ppIF-derived V_Ts were strongly correlated with original ppIF-derived V_Ts derived from compartmental modelling (Additional file 1).

Voxelwise SUVs

SUV images (see [11]) were calculated for all 10-min epochs from 20–30 to 80–90 min from decay-corrected summation images, using MICKPM (version 5.4 software, running in MATLAB (The MathWorks Inc., Cambridge, UK)). "MICKPM" (Modelling, Input functions and Compartmental Kinetics—Parametric Maps) is a quantitative PET analysis software that is available on request from Rainer Hinz (Wolfson Molecular Imaging Centre, University of Manchester; rainer.hinz@manchester.ac.uk). Epochs of 30–60 and 60–90 min were also tested, but yielded very similar results (data not shown).

PBIFs

The generation of PBIFs can be split into "magnitude normalisation" and "scaling" stages, described below.

After controlling for weight and injected dose, we identified a near-significant ($p = 0.08$) negative ($r = -0.66$) correlation between age and area under the parent fraction curve. We therefore incorporated this additional variable into the method used to generate the "magnitude normalised" input functions: (1) normalisation of participants' ppIFs according to weight, then injected dose, then age (multiplying each participant's ppIF according to the ratio [median value/participant value]); (2) alignment of each ppIF peak to peak at 80 s; and (3) calculation of the median (i.e. standardised) ppIF from the 19 ppIFs.

In order to generate individualised PBIFs, the median ppIF was scaled as follows: (1) linear regression of the area under the 19 other participants' ppIF curves (AUCs) with the parent radioactivity concentration in plasma at 90 min post-injection (assumed equivalent to venous plasma [14]) and then (2) scaling of the median ppIF according to the ratio of the AUC predicted (according to the linear regression) by the parent radioactivity concentration in the participant's arterial plasma at 90 min to the AUC of the median ppIF.

Our PBIF method depended on a single parent plasma sample. Other approaches to scaling, i.e. according to injected dose and/or body mass (kg) alone or in combination, were found to yield weaker correlations with original ppIF-derived V_Ts (data not shown).

The PBIFs were used to perform voxelwise SA, as above.

Scan shortening

Voxelwise SA was performed using the original ppIFs and dynamic emission data over $t = 0–60$, t = 0–70 min,

and $t = 0–80$ min, using slow component boundaries of 0.000290, 0.000256, and 0.000222 s^{-1}, respectively.

Statistical analyses

We calculated the mean (original ppIF derived or PBIF derived, as applicable) V_T/SUV within seven cortical and subcortical bilateral ROIs using Analyze 7.0 (AnalyzeDirect Inc., Kansas, USA): cerebelli, hippocampi, occipital lobes, occipito-temporal (fusiform) gyri, parahippocampal gyri, putamina, superior frontal gyri (SFG), and thalami. Correlations were interrogated using Spearman's rank coefficient. Pooled correlations were quantified using 140 data points (20 participants × seven ROIs) per variable. Original ppIF-derived and PBIF-derived V_Ts, and separately original ppIF-derived V_Ts that were calculated using 90- or 60-min datasets, were compared using Bland–Altman plots. Binding estimates were compared between subgroups [6] (epilepsy not on antidepressants, epilepsy on antidepressants, controls) by multivariate analysis of variance, with age as a covariate; a significant effect ($p = 0.007$ overall; individual ROIs $p < 0.001$) of subgroup on original ppIF-derived 90-min V_Ts was already reported [6].

Results

Voxelwise SUVs

SUVs were correlated with 90-min original ppIF-derived V_Ts derived from SA (seven ROIs pooled: increasing with time and reaching a maximum of $\rho = 0.78$ for 80–90 min; all $p < 0.001$; Fig. 1; Additional file 1).

The ranges of ρ were 0.34 (SFG) to 0.60 (cerebelli) for the interval 10–20 min, and 0.65 (hippocampi) to 0.79 (cerebelli and occipital lobes; all $p \leq 0.001$) for the interval 80–90 min.

There was very little difference (< 1.3 percentage points) in the ROI between-subject coefficients of variation (BS-CVs) between the 80–90 min SUVs and the original ppIF-derived V_Ts (Additional file 1: Table S1). Larger differences were seen using earlier intervals.

The influence of subgroup on original ppIF-derived V_T [6] was not replicated for SUV data ($p \geq 0.05$ for each interval).

PBIFs

PBIF-derived V_Ts were correlated with V_Ts calculated using the participants' original ppIFs (seven ROIs pooled $\rho = 0.90$, $p < 0.001$). A small bias toward overestimation of PBIF-derived V_T was observed (linear regression $y = 1.02x - 0.20$; see Fig. 2) with a large variability (mean overestimate 0.7% ± 13.4%).

The range of ρ was 0.81 (hippocampi and occipital lobes) to 0.92 (cerebelli; all $p < 0.001$; see Additional file 1: Table S2). The absolute percent difference between PBIF-derived V_Ts and those calculated using the participants' original ppIFs varied somewhat unpredictably across ROIs (Fig. 2), but was worse for elderly, healthy control participants.

An increase in BS-CV was observed that ranged from 2.5 percentage points (SFG) to 4.1 percentage points (occipital lobes; see Additional file 1: Table S2), i.e. mean ± standard deviation BS-CV was 26 ± 2% compared to 23 ± 2% for original ppIF-derived V_Ts.

The influence of subgroup on original ppIF-derived V_T [6] was not replicated for PBIF-derived V_Ts ($p = 0.11$).

Scan shortening

ROI original ppIF-derived V_Ts calculated using 60-, 70-, and 80-min datasets were positively correlated with

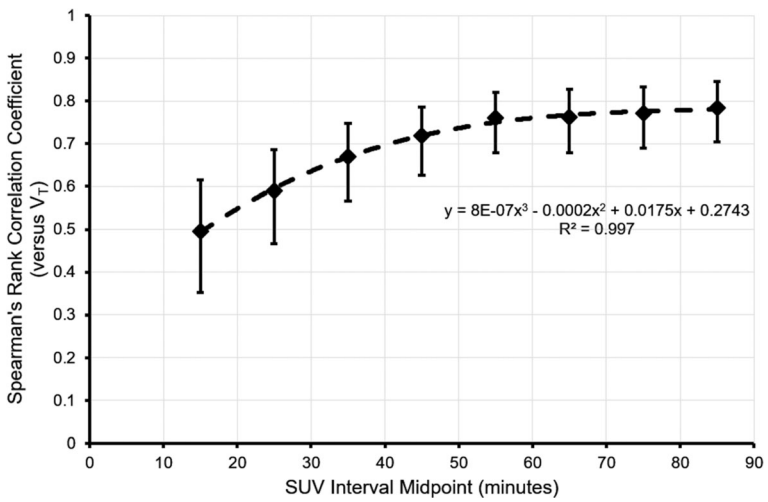


Fig. 1 Spearman's rank correlation coefficient versus the midpoint of the SUV interval. The correlation coefficient refers to SUV versus original ppIF-derived V_T for seven ROIs pooled. Error bars indicate 95% confidence intervals

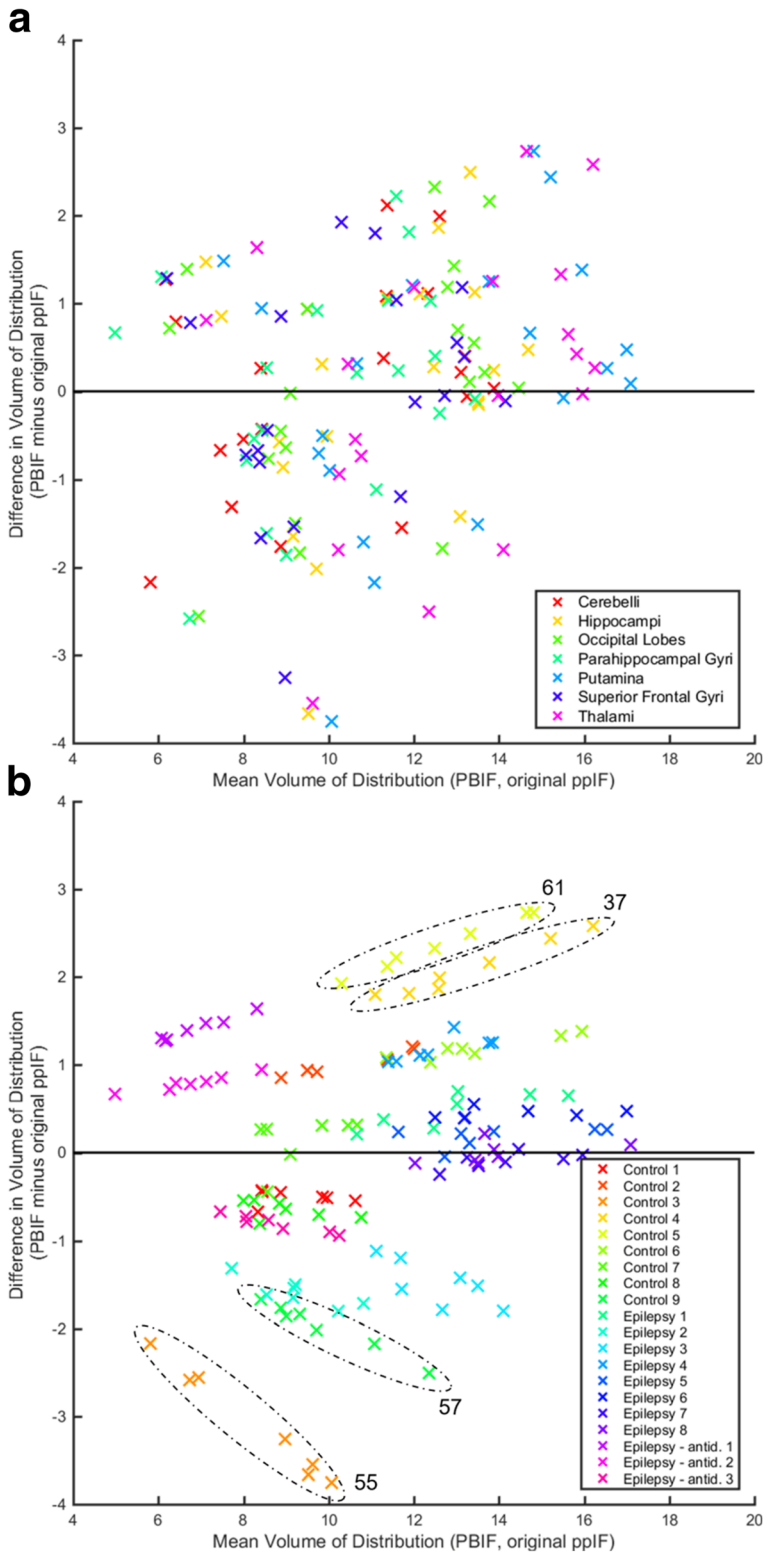


Fig. 2 Bland–Altman plot for V_T calculated using PBIFs versus using the original ppIFs. V_Ts were calculated using 90-min datasets. The colour scale depicts ROI (**a**, top) or participant identification (**b**, bottom). The dash ovals identify participants with large differences in V_T, with their age in years (the median age of participants was 35 years, interquartile range 26–50 years, range 20–62 years). antid., on antidepressants

Table 1 Original ppIF-derived V_T calculated over various intervals versus original ppIF-derived V_T calculated using the 90-min datasets, via voxelwise SA

	0–60 min			0–70 min			0–80 min			0–90 min
	Mean ± SD	ρ	%	Mean ± SD	ρ	%	Mean ± SD	ρ	%	Mean ± SD
Cerebelli	9.3 ± 2.4	1.00	− 6.7	9.6 ± 2.5	1.00	− 4.4	9.8 ± 2.5	1.00	− 2.2	10.0 ± 2.5
Hippocampi	9.6 ± 1.8	0.98	− 14.1	10.2 ± 2.0	0.99	− 9.0	10.8 ± 2.1	1.00	− 3.9	11.2 ± 2.2
Occipital lobes	9.9 ± 2.4	0.98	− 8.3	10.2 ± 2.5	0.98	− 5.1	10.5 ± 2.5	1.00	− 2.4	10.7 ± 2.5
Parahippocampal gyri	8.5 ± 2.0	0.98	− 13.8	9.0 ± 2.1	0.99	− 8.8	9.5 ± 2.2	0.99	− 4.1	9.9 ± 2.3
Putamina	11.7 ± 2.6	0.99	− 7.3	12.1 ± 2.7	1.00	− 4.7	12.4 ± 2.8	1.00	− 2.2	12.7 ± 2.9
Superior frontal gyri	9.4 ± 2.2	0.97	− 8.2	9.7 ± 2.3	0.98	− 5.5	10.0 ± 2.3	0.99	− 2.7	10.3 ± 2.3
Thalami	11.4 ± 2.4	0.97	− 10.1	11.9 ± 2.6	0.98	− 6.2	12.3 ± 2.6	0.99	− 2.9	12.7 ± 2.7
Seven pooled ROIs	**10.0 ± 2.5**	**0.98 CI (0.97–0.99)**	**− 9.8**	**10.4 ± 2.6**	**0.99 CI (0.98–0.99)**	**− 6.2**	**10.7 ± 2.6**	**1.00 CI (1.00–1.00)**	**− 2.9**	**11.1 ± 2.7**

% mean percentage difference, relative to 90-min SA original ppIF-derived V_T; ρ Spearman's rank correlation coefficient; *CI 95%* confidence interval; *SD* standard deviation

original ppIF-derived V_Ts derived from the full 90-min dataset (seven ROIs pooled $\rho = 0.98$, $\rho = 0.99$, and $\rho = 1.00$ respectively; all $p < 0.001$; Table 1, Fig. 3).

Correlation coefficients ranged from 0.97 (SFG and thalami, 60 min) to 1.00 (multiple ROIs and scan durations; all $p < 0.001$). The original ppIF-derived V_T was increasingly underestimated (relative to original ppIF-derived V_Ts calculated using 90-min datasets) with scan shortening, particularly for medial temporal lobe ROIs (Table 1, Fig. 4).

There was very little difference (< 0.9 percentage points) in ROI BS-CVs between the shortened original ppIF-derived V_Ts and the original ppIF-derived 90-min V_Ts.

The influence of subgroup on original ppIF-derived V_T [6] was replicated using all shortened datasets: 60 min ($p = 0.001$), 70 min ($p = 0.003$), and 80 min ($p = 0.005$).

Discussion

We report further analyses of [^{18}F]GE-179 PET datasets to facilitate wider use of the radiotracer. Our major findings are (1) SUVs were correlated with 90-min original ppIF-derived V_Ts; (2) PBIF-derived V_Ts were more strongly correlated with original ppIF-derived V_T estimates but had increased BS-CV; (3) original ppIF-derived V_Ts calculated over 60+ min were very strongly correlated with 90-min original ppIF-derived V_Ts, but with negative bias; and (4) we were able to replicate our original findings using the original ppIF-derived V_Ts derived from shortened datasets, but not using SUVs or PBIF-derived V_Ts.

While SUVs were only moderately correlated with original ppIF-derived V_Ts, the correlation coefficients started to plateau over later intervals, i.e. from 50 to 60 min onwards (see Fig. 1 and Additional file 1: Table S1). Our data suggest any increase in correlation

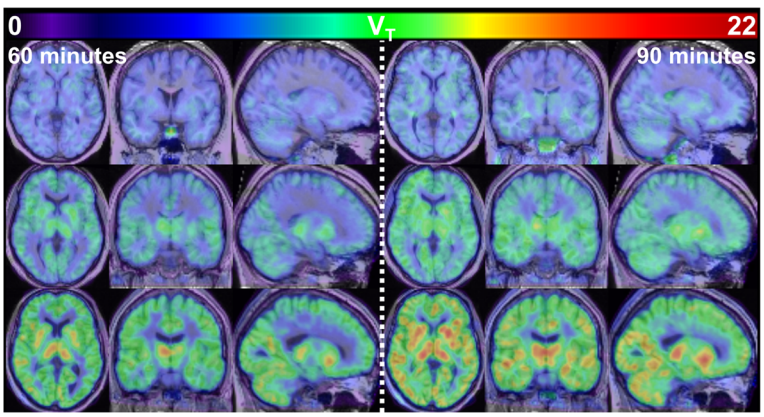


Fig. 3 Original ppIF-derived V_T images calculated using 60-min (left panel) and 90-min (right panel) datasets. Colour scale—original ppIF-derived V_T; top row—participant with epilepsy on antidepressants (epilepsy—antid. 2); middle row—control participant (control 2); bottom row—participant with epilepsy, not on antidepressants (epilepsy 5). Images are shown in radiological orientation

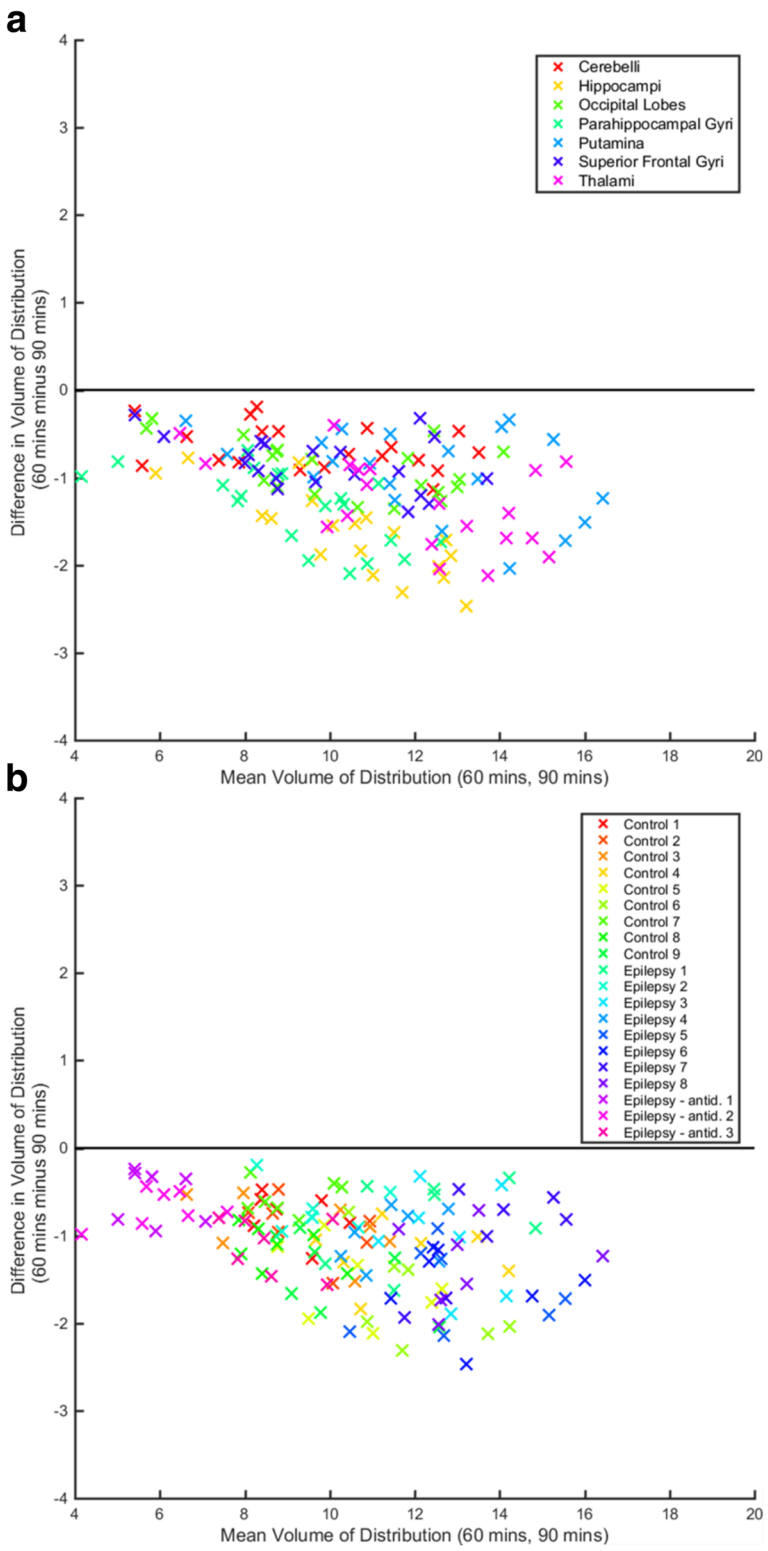


Fig. 4 Bland–Altman plot for 60 min' original pplF-derived V_T versus 90 min' original pplF-derived V_T. The colour scale depicts ROI (**a**, top) or participant identification (**b**, bottom). antid., antidepressants; mins, minutes

coefficient achieved by delaying SUVs to scanning intervals beyond 90 min is likely to be modest.

PBIFs, whether scaled by injected dose, body mass, whole-blood, or plasma radioactivity, performed somewhat unpredictably across ROIs and inconsistently across participants. Although normalisation by age is not a standard approach, in practice, it had a small effect on the standardised ppIF (median difference ~ 5.5%; data not shown) which for example translated into a 0.8% difference in global PBIF-derived [^{18}F]GE-179 V_T. Hence, we do not believe the age normalisation procedure had a strong bearing on the results.

Where arterial blood sampling is not available, calculation of SUVs constitutes a convenient alternative with fewer outliers than the PBIF methods. However, we were unable to replicate our original finding of differences between subgroups using SUVs.

We deliberately employed a simple PBIF method that could be widely implemented. A novel method was recently described that allows simultaneous estimation of the kinetic rate constants and the input function parameters from emission data alone [15]. However, it requires a priori specification of the number of tissue compartments and can yield a similar margin of error to what we found for PBIFs [15].

It was not possible to test image-derived input functions with our data which had a limited field of view. We also could not test PBIFs anchored via venous blood samples.

Our findings suggest that where arterial blood sampling is available, it is possible to shorten the scan to 60, 70, or 80 min, without adversely affecting BS-CV or study power. However, investigators should be aware of the negative bias, which is more pronounced in the medial temporal lobe.

Additional file

Additional file 1: Voxelwise spectral analysis (SA) versus the two-tissue compartment model (2c4kbv), voxelwise SUVs calculated overall various intervals, and PBIF-derived V_Ts. (PDF 1382 kb)

Acknowledgements
We thank the staff of Hammersmith Imanet Limited and the Epilepsy Society MRI Unit for their assistance with the data acquisition. We are very grateful to the anonymous reviewers, whose comments helped us to improve the quality of this manuscript.

Funding
The initial study was supported by the Medical Research Council (MRC) Clinical Sciences Centre and GE Healthcare Ltd. CJM was supported by a MRC Doctoral Training Account studentship that was awarded by Imperial College London; he is currently supported by MRC grant MR/N013042/1. JSD and MJK were supported by an MRC-DPFS grant (MR/L013215/1), Epilepsy Society, UCL, UCL Hospitals, and UCLH/UCL Biomedical Research Centre. AH was supported by an MRC Clinician Scientist Fellowship (G108/585) and the Neurodis Foundation.
WT was an employee of GE Healthcare Ltd. CJM, JSD, and MJK have received fees from GE Healthcare Ltd. but have never been employees of the organisation.

Availability of data and materials
The authors have submitted all major results from the study for publication. Unpublished datasets supporting the conclusion of this article are only available to the investigators at present. Any request for data can be addressed to the corresponding author; any data sharing will be subject to restrictions based on anonymisation rules.

Authors' contributions
In the initial study, CJM, WT, DJB, JSD, and MJK contributed to the conception and design; CJM, DARB, WT, and JSD contributed to the data acquisition; and CJM, WT, JSD, MJK, and AH contributed to the data analysis and interpretation. In the present study, CJM and AH contributed to the conception and design; CJM, WT, DJB, RH, MJK, JSD, and AH contributed to the data analysis and interpretation; and CJM, DARB, WT, DJB, RH, JSD, MJK, and AH contributed to the manuscript preparation and revision. All authors read and approved the final manuscript.

Ethics approval and consent to participate
We confirm that Ethics Committee (Royal Marsden, reference number 09/H0801/79) and other regulatory approvals were obtained prior to initiation of the study, as detailed in [2, 6]. All participants provided written, informed consent prior to participation.

Competing interests
The initial study was supported in part by GE Healthcare Ltd., who developed the radiotracer, [^{18}F]GE-179. WT was an employee of GE Healthcare Ltd. CJM, JSD, and MJK have received fees from GE Healthcare Ltd. but have never been employees of the organisation. JSD has also received fees from UCB Pharma, Eisai, and GSK. The remaining authors declare that they have no competing interests.

Publisher's Note
Springer Nature remains neutral with regard to jurisdictional claims in published maps and institutional affiliations.

Author details
[1]Division of Brain Sciences, Imperial College London, London, UK. [2]MRC Clinical Sciences Centre, London, UK. [3]School of Biomedical Engineering and Imaging Sciences, King's College London, 4th Floor Lambeth Wing, St Thomas' Hospital, Westminster Bridge Road, London SW1 7EH, UK. [4]King's College London and Guy's and St Thomas' PET Centre, St. Thomas' Hospital, London, UK. [5]GE Healthcare Ltd, Buckinghamshire, UK. [6]Department of Nuclear Medicine, Aarhus University, Aarhus, Denmark. [7]Institute of Neuroscience, University of Newcastle, Newcastle upon Tyne, UK. [8]Wolfson Molecular Imaging Centre, University of Manchester, Manchester, UK. [9]Department of Clinical and Experimental Epilepsy, UCL Institute of Neurology, London, UK. [10]Epilepsy Society, Buckinghamshire, UK. [11]The Neurodis Foundation, CERMEP—Imagerie du Vivant, Lyon, France.

Received: 7 March 2018 Accepted: 8 May 2018
Published online: 11 June 2018

References
1. Kalia LV, Kalia SK, Salter MW. NMDA receptors in clinical neurology: excitatory times ahead. Lancet Neurol. 2008;7(8):742–55.
2. McGinnity CJ, Hammers A, Riaño Barros DA, Luthra SK, Jones PA, Trigg W, et al. Initial evaluation of ^{18}F-GE-179, a putative PET tracer for activated N-methyl D-aspartate receptors. J Nucl Med. 2014;55(3):423–30.
3. Ahmed I, Bose SK, Pavese N, Ramlackhansingh A, Turkheimer F, Hotton G, et al. Glutamate NMDA receptor dysregulation in Parkinson's disease with dyskinesias. Brain. 2011;134(Pt 4):979–86.
4. Schoenberger M, Schroeder FA, Placzek MS, Carter RL, Rosen BR, Hooker JM, et al. In vivo [^{18}F]GE-179 brain signal does not show NMDA-specific modulation with drug challenges in rodents and nonhuman primates. ACS Chem Neurosci. 2018;9(2):298–305.
5. Yang J, Zorumski CF. Effects of isoflurane on N-methyl-D-aspartate gated ion channels in cultured rat hippocampal neurons. Ann N Y Acad Sci. 1991;625:287–9.
6. McGinnity CJ, Koepp MJ, Hammers A, Riaño Barros DA, Pressler RM, Luthra S, et al. NMDA receptor binding in focal epilepsies. J Neurol Neurosurg Psychiatry. 2015;86(10):1150–7.

7. Spinks TJ, Jones T, Bloomfield PM, Bailey DL, Miller M, Hogg D, et al. Physical characteristics of the ECAT EXACT3D positron tomograph. Phys Med Biol. 2000;45(9):2601–18.
8. Heckemann RA, Keihaninejad S, Aljabar P, Rueckert D, Hajnal JV, Hammers A. Improving intersubject image registration using tissue-class information benefits robustness and accuracy of multi-atlas based anatomical segmentation. NeuroImage. 2010;51(1):221–7.
9. Heckemann RA, Hajnal JV, Aljabar P, Rueckert D, Hammers A. Automatic anatomical brain MRI segmentation combining label propagation and decision fusion. NeuroImage. 2006;33(1):115–26.
10. Defrise M, Kinahan PE, Townsend DW, Michel C, Sibomana M, Newport DF. Exact and approximate rebinning algorithms for 3-D PET data. IEEE Trans Med Imaging. 1997;16(2):145–58.
11. McGinnity CJ, Riaño Barros DA, Rosso L, Veronese M, Rizzo G, Bertoldo A, et al. Test-retest reproducibility of quantitative binding measures of [^{11}C]Ro15-4513, a PET ligand for GABAA receptors containing alpha5 subunits. NeuroImage. 2017;152:270–82.
12. Cunningham VJ, Jones T. Spectral analysis of dynamic PET studies. J Cereb Blood Flow Metab. 1993;13(1):15–23.
13. Turkheimer FE, Brett M, Visvikis D, Cunningham VJ. Multiresolution analysis of emission tomography images in the wavelet domain. J Cereb Blood Flow Metab. 1999;19(11):1189–208.
14. Hahn A, Nics L, Baldinger P, Ungersbock J, Dolliner P, Frey R, et al. Combining image-derived and venous input functions enables quantification of serotonin-1A receptors with [carbonyl-^{11}C]WAY-100635 independent of arterial sampling. NeuroImage. 2012;62(1):199–206.
15. Zanderigo F, Ogden RT, Parsey RV. Noninvasive blood-free full quantification of positron emission tomography radioligand binding. J Cereb Blood Flow Metab. 2015;35(1):148–56.

Submit your manuscript to a SpringerOpen journal and benefit from:

► Convenient online submission
► Rigorous peer review
► Open access: articles freely available online
► High visibility within the field
► Retaining the copyright to your article

Submit your next manuscript at ► springeropen.com